Effect of the reactants concentration on the synthesis and cycle life of copper hexacyanoferrate for aqueous Zn-ion batteries

Giorgia Zampardi [a,*], Michael Warnecke [a], Michele Tribbia [a], Jens Glenneberg [b], Cleis Santos [a], Fabio La Mantia [a,b,*]

[a] *Universität Bremen, Energiespeicher- und Energiewandlersysteme, Bibliothekstraße 1, 28359 Bremen, Germany*
[b] *Fraunhofer Institute for Manufacturing Technology and Advanced Materials, IFAM, Wiener Str. 12, 28359, Bremen, Germany*

ARTICLE INFO

ABSTRACT

Copper hexacyanoferrate (CuHCF) is a promising Zn^{2+} insertion material as positive electrode in mild aqueous Zn-ion batteries for power grid applications, due to its excellent power capability, non-toxicity, low cost and easy synthesis route. Here, the effect of the reactants' concentration and ratio during the synthesis of the CuHCF on the performance of the resulting material has been investigated through morphological, crystallographic and compositional analysis. Despite the different reaction's conditions, the synthesised CuHCF powders did not show any significant change in their average particle size and morphology. Nevertheless, different structural and compositional characteristics have been observed for the different samples. In particular, different amounts of potassium have been found in the crystal structure of the investigated CuHCF materials. Subsequent electrochemical analysis demonstrated that the CuHCF with higher initial potassium content showed higher stability and therefore achieved longer cycle life.

1. Introduction

In recent years, aqueous Zn-ion batteries (ZIBs) have attracted great attention because of their applicability as cheap and environmentally friendly energy storage devices for power grid applications [1–4]. Beside the optimization of the electrodeposition efficiency of the metallic zinc occurring at the negative electrode [5,6], research is focused in finding an active material for the positive electrode having long cycle life, and appropriate energy density and power capability [2,7–10]. Belonging to the Prussian blue analogues (PBAs) family, copper hexacyanoferrate (CuHCF) has been shown to be a promising candidate as positive electrode material for aqueous ZIBs. Due to its high average working potential (c.a. 1.7 V vs Zn/Zn^{2+}) and its excellent power rate capability, together with low toxicity and costs, it is suitable for power grid applications [7,8,11]. Moreover, CuHCF can be synthesised through a facile synthesis route, which makes its industrial scaled-up production feasible [2].

Despite CuHCF can be produced through an easy co-precipitation route, the synthesis of the desired phase is not straightforward to control [1,2,11,12]. Such complications in controlling the synthesis' reaction mechanism are commonly shared by the whole family of Prussian

Blue analogues, because of the intrinsic challenge related to accurately control the process of the particles' nucleation and growth. As a matter of facts, several parameters (such as: reaction time and temperature, reactants' concentration, thermal treatments, etc.) can affect the resulting material phase(s), particles dimension and shape, ion and water content in the crystal, etc., strongly influencing the material performance [1,2,12,13]. As an example, zinc hexacyanoferrate (ZnHCF) has been synthesised with different particle shapes, namely cubo-octahedron, truncated octahedron and octahedron, by simply changing the mixing times of the reactants-containing solutions [1,12]. These different morphologies showed different electrochemical performance during the Zn^{2+} (de-)insertion: the cuboctahedral particles had the highest charge capacity (of c.a. 68 mAh g^{-1}) among the three morphologies, probably because of a better diffusion of the Zn^{2+} ions within the lattice channels [1,12].

It follows that a deeper understanding of the effects of the synthesis parameters may result in synthesising PBAs with improved performance, with clear benefits to the aqueous ZIBs optimisation. In particular, as the processes governing the stability of the CuHCF and its ageing mechanism remain not clearly understood [14,15], a more careful control of the synthesis may lead to the identification of the parameters that

---

dictate the stability of CuHCF. Such understanding may allow the synthesis of a CuHCF reaching a cycle life of 2000–3000 cycles at current rate of 1C, which is a realistic operational current rate for power grid applications.

For this reason, in the frame of this work the effect of the reactants' concentration within the precursor solutions on the electrochemical behaviour of the resulting CuHCF has been investigated. CuHCF powders have been synthesised from five different starting solutions with the two reactants $Cu(NO_3)_2$ and $K_3Fe(CN)_6$ having different concentrations and ratios. Crystallographic, morphological and compositional characterisations have been performed on the resulting pristine CuHCF powders. Successively, electrochemical analysis through galvanostatic cycling and differential charge plots has been carried out in order to estimate the Zn^{2+} (de-)insertion behaviour of the different in-house synthesised CuHCF powders.

2. Experimental

2.1. Materials synthesis

CuHCF was synthesised through the routinely employed co-precipitation method [7,8,11]. Depending on the synthesis, two solutions of $Cu(NO_3)_2 \cdot 3H_2O$ (Sigma Aldrich) and $K_3Fe(CN)_6$ (Sigma Aldrich) with different concentrations (Table 1) were simultaneously added dropwise to 60 ml of deionised water under vigorous stirring at room temperature. The suspension was sonicated for 30 min, and left to settle overnight. The resulting precipitate was centrifuged, rinsed with 1 M KNO_3 (Sigma Aldrich) and 10 mM HNO_3 (Sigma Aldrich) and then dried at 60 °C overnight. The dry powder was then ground with mortar and pestle.

2.2. Materials characterisation

All electrochemical measurements have been carried out with the aid of a Biologic VMP3 potentiostat, in flooded three-electrode electrochemical cells consisting of: CuHCF-based paste electrode as working electrode, zinc foil (99.99% Good Fellow) as counter electrode, and an in-house assembled Ag/AgCl reference electrode (3 M KCl, E_{RE} = + 0.210 V vs. SHE) separated by the electrolyte through a ceramic frit. The electrolyte consisted of 100 mM $ZnSO_4$ (Sigma Aldrich). The CuHCF-based electrodes were prepared by hand painting the slurry on a carbon cloth current collector (Fuel Cell Earth). The electrode slurry consisted of in-house synthesised CuHCF, conductive additive (Super C65, Timcal), Polyvinylidene fluoride (PVdF, Solef S5130-Solvay) and graphite (SFG6, Timcal) dispersed in N-methyl-2-pyrrolidone (NMP, Sigma-Aldrich) with a wt.% ratio of 80:9:9:2. The slurry was mixed with the aid of an Ultra-Turrax disperser (IKA) for 30 min at 4000 rpm. The mass loading of the resulting CuHCF-electrodes was of c.a. 10 mg cm^{-2} of active material. When shown within the graphs, the average and standard deviation have been calculated by comparing at least two different samples resulting from two different synthesis-batches for

every synthesised material. All the CuHCF-based electrodes have been galvanostatically cycled with a current density of 85.2 mA g^{-1}, corresponding to a C-rate of 1C.

The x-ray powder diffraction (XRPD) patterns of the pristine CuHCF powders have been obtained between 10° and 50° in the 2θ range through a Miniflex Rigaku® diffractometer for powder analysis by using CuKα radiation. The step size was 0.03° with a scan speed of 5 sec/step. For every analysis, the powder sample was placed on the quartz holder without using any solvent. Every diffractogram was normalised using the intensity of its highest peak. The resulting plot was indexed with a F-centred cubic unit cell. Microstructural and morphological analysis was performed via scanning electron microscopy (SEM), using a FEI Helios NanoLab™ 600 DualBeam™ apparatus. Here, due to the insufficient electronic conductivity of the particles, the backscattered electron mode was employed using an acceleration voltage of 15 kV, and a beam current of 0.69 nA. Additionally, compositional information of the respective pristine powders was acquired with the help of energy dispersive x-ray spectroscopy (EDX) employing the same beam parameters.
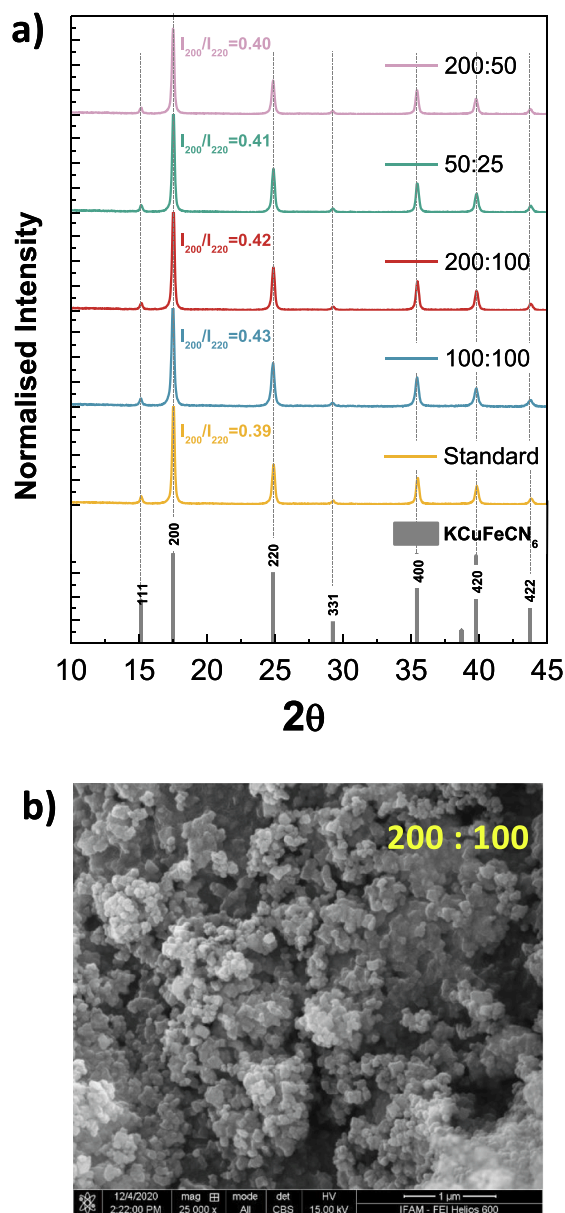
3. Results and discussion

At first, different copper hexacyanoferrate (CuHCF) powders have been synthesised with employing reactants-containing solutions having different concentrations, as summarised in Table 1. The standard CuHCF co-precipitation synthesis is routinely performed in excess copper with the two reactants $Cu(NO_3)_2$ and $K_3Fe(CN)_6$ having a ratio of 2:1 and a concentration of 100 mM and 50 mM, respectively (CuHCF 100:50) [11]. Here, as shown in Table 1, the standard reactants ratio (2:1) has been kept for the samples 200:100 and 50:25, but the reactants concentration has been increased and decreased twofold, respectively. At constant reaction's yield, an increase in the reactants' concentration would reduce the reaction volumes (or at constant reaction volumes, it would increase the reaction yield), and therefore would be desirable for an industrial scaled-up production of the CuHCF. On the contrary, a diluted concentration of the reactants might favour the formation of a different particles' size/morphology [1,12]. As routinely the CuHCF is synthesised with excess of Cu (2:1 respect to K), a material with increased 4:1 ratio between the two reactants has been synthesised as well, namely the 200:50 CuHCF, in order to verify if a stronger excess of copper during the CuHCF synthesis would result in a more efficient material. Lastly, a synthesis with the reactants ratio of 1:1 has been performed as well (100:100), as avoiding to work with excess copper would reduce the CuHCF production costs (being $Cu(NO_3)_2$ the most expensive chemical needed during the synthesis of the CuHCF).

After synthesising all the different CuHCF powders, XRPD patterns have been taken from the pristine powders (Fig. 1a) showing that a similar highly crystalline material has been obtained as a result of the different synthesis employing different reactants' concentrations. In particular, the main reflections in the pattern corresponded to the main reflections of $K_{2x/3}Cu[Fe(CN)_6]_{2/3} \cdot nH_2O$, which is characterised by a cubic framework (space Fm3m) [16]. Such crystal structure containing

Table 1

Summary of the concentration of the reactant-containing solutions used for the different synthesis of CuHCF, normalised K-to-Fe and Cu-to-Fe ratios, average particles' dimension and I_{220}/I_{200} peak intensity for all the pristine CuHCF powders, including the average maximum discharge capacity and energy at the 25th cycle. (The average maximum discharge capacity and energy have been estimated by considering at least two CuHCF-based electrodes prepared with CuHCF powders coming from two synthesis' batches.)

Synthesis	$Cu(NO_3)_2 : K_3Fe(CN)_6$ Concentration [mM]	K : Cu : Fe Normalised Ratios to Fe	Average Particles Diameter[nm]	I_{220}/I_{200} Peak Intensity Ratios	Average $Q_{discharge}$ @25° cycle [mAh g^{-1}]	Average Energy$_{discharge}$ @25° cycle [mWh g^{-1}]
50:25	50:25	0.04:1.52:1	66 ± 20	0.41	53 ± 1.0	86 ± 1.8
Standard	100:50	0.03:1.58:1	68 ± 16	0.39	56 ± 1.3	92 ± 2.4
200:100	200:100	0.06:1.56:1	83 ± 25	0.42	58 ± 0.1	94 ± 2.6
100:100	100:100	0.09:1.50:1	57 ± 13	0.43	56 ± 0.9	92 ± 2.0
200:50	200:50	0.02:1.54:1	65 ± 16	0.40	60 ± 2.0	102 ± 1.2

Fig. 1. a) XRPD patterns of the pristine CuHCF powders synthesised with different $Cu(NO_3)_2$ and $K_3Fe(CN)_6$ concentrations; the vertical lines correspond to the simulated patterns of the $KCuFe(CN)_6$ reported in reference [16]; b) SEM image of the pristine CuHCF powder synthesised with the $Cu(NO_3)_2$: $K_3Fe(CN)_6$ concentration of 200 mM : 100 mM.

Fe^{III} octahedrally linked with the CN^- groups, generates the open framework structure with large channels available for the (de-)insertion of guest ions, which is a typical trait of the PBAs family [2,17–19].

Despite the similarities of the XRPD patterns, a change in the I_{200}/I_{220} peak intensity ratio could be observed among the different samples (Fig. 1a and Table 1). Additionally, a shift towards higher 2-theta of the (200) reflection was observed for the 100:100, 200:100 and, 50:25 CuHCF samples with respect to the standard one (100:50), whereas 200:50 remained at the same 2θ. SI Section 1 shows the 2θ shifts of the (200) and (220) reflections. As pointed out by Ojwang et al., both the increase in the I_{200}/I_{220} peak intensity ratios and such 2θ shift can be explained with the presence of potassium ions within the CuHCF structure [16,20]. Here, the variation of the synthesis conditions (i.e. the change of the ratio/concentration of the two reactants $Cu(NO_3)_2$ and $K_3Fe(CN)_6$) caused a slight modification of the composition of the resulting CuHCF crystal structure. In particular, a higher I_{200}/I_{220} peak

intensity ratio and a shift towards higher 2θ, which are symptomatic of a higher amount of K ion within the CuHCF lattice, indicates smaller unit-cell parameters. When K ions are present within the CuHCF structure, the Cu–N bond distance of the lattice is slightly reduced, thus affecting the electronic structure of the Fe in the crystal [16,20]. According to the XRPD patterns, the CuHCF particles exhibiting a higher K-content in their lattice were the 200:100 and especially the 100:100, which are the powders characterised by the highest I_{200}/I_{220} peak intensity ratio and the most prominent shift towards higher 2θ (Table 1, SI Section 1).

All the CuHCF powders exhibited no significant difference in terms of average particles diameter (around 60–80 nm) and morphology as the one shown in Fig. 1b (see also Table 1 and SI Section 2 for the SEM images and the distribution of the particles' size for all the CuHCF powders). Through EDX analysis, a similar normalised Cu-to-Fe atomic ratio of c.a. 1.5 has been observed for all the pristine CuHCF materials, whilst their K-content changed with changing the reactants concentration. In particular, the 200:100 and especially the 100:100 CuHCF were characterised by the higher normalised K-to-Fe ratios of 6% and 9%, respectively as shown in Table 1. The complete compositional analysis of all the pristine powders can be found in SI Section 3. It is worth noticing that in order to reduce the experimental errors in the EDX analysis correlated to the samples' preparation and handling, all the samples have been carefully prepared in the same way, having the same orientation with respect to the EDX detector. The fact that the compositional analysis is supported with what has been observed through the XRPD pattern analysis due to the different I_{200}/I_{220} peak intensity ratios and the (200) reflection shift towards higher 2θ values, is a further evidence of the higher initial K-content of the 200:100 and especially 100:100 CuHCF powder.

Subsequently, the CuHCF-based electrodes have been galvanostatically cycled at a rate of 1C in an aqueous solution containing 100 mM $ZnSO_4$. All the different CuHCF electrodes showed a similar initial capacity (Table 1), however their cycle life varied significantly in dependence on the reactants' concentration employed during their synthesis. In particular, the 200:100 and the 100:100 CuHCF reached a capacity retention of 80% after 475 and 600 cycles respectively, contrary to the standard CuHCF (100:50) reaching 80% of capacity retention after 250–300 cycles (Fig. 2a). In agreement with what has been previously reported on this material [7,21], all the CuHCF-based electrodes showed a very high coulombic efficiency (>99%), independently on the synthesis conditions. In particular, as shown in Fig. 2b, the average coulombic efficiency ranged between 99.4% and 99.7% among the different CuHCF-based electrodes.

The average energy that the cell could deliver during its discharge has been calculated considering an ideal Zn counter electrode ($E_{Zn/Zn2+}$ = −1.025 V vs Ag/AgCl), and despites its initial value did not change substantially (Table 1), its retention varied significantly among the different CuCHF electrodes. Similarly, the cells with the 200:100 and 100:100 CuHCF-based electrodes reached the 80% of energy retention after 550 and 800 cycles, respectively, whilst the one containing the standard CuHCF (100:50) only after 300 cycles (Fig. 2c).

Such extended cycle life when considering the average delivered energy of the cell with respect to the capacity of the electrode is related to the change of the galvanostatic profile of the CuHCF during the cycling from a single-phase to a two-phase one, with the development of a plateau at c.a. 0.8 V vs. Ag/AgCl [11]: during its ageing, the specific capacity loss of the material is therefore conveniently compensated, at least partially, by an increase in Zn^{2+} (de-)insertion potential. As shown in Fig. 3a, 3b, both the 200:100 and 100:100 CuHCF develop such higher-potential plateau in a more pronounced way along the galvanostatic cycles with respect to the standard CuHCF (100:50, Fig. 3c) and to the other synthesised CuHCF-powders as well (SI Section 5). This is even more evident in the differential charge plots, in which the development of the plateau in the galvanostatic cycles corresponds to the development of two new peaks located around 0.8 V vs. Ag/AgCl (Fig. 3d, 3e, 3f). As previously reported, such pair of newly developed peaks are
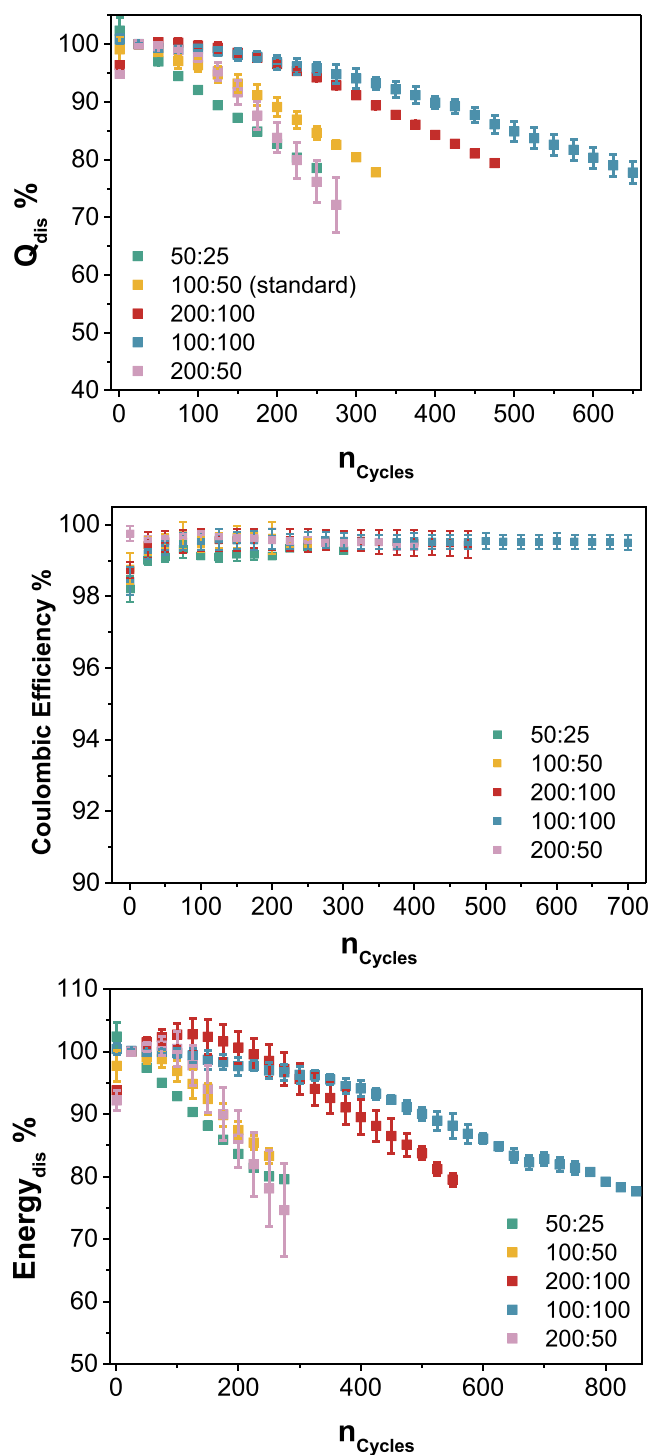
Fig. 2. Average a) charge and c) energy retention together with the average b) coulombic efficiency of the different CuHCF-based electrodes galvanostatically cycled at 1C. Both retentions have been normalised by the charge/energy at the 25th cycle. The average and standard deviation have been calculated by comparing at least two different samples resulting from two different synthesis-batches for every synthesised CuHCF.

related to the phase transition occurring during the ageing of the CuHCF [7,11]. It has been previously suggested that such phase transition may involve a partial substitution of Cu^{2+} with Zn^{2+} in the B sites of the CuHCF crystal, with the consequent formation of a distorted CuZnHCF phase [7,11]. Moreover, such phase transition with consequent change of the potential profile may also be due to the formation of a different

insertion site, with the Zn^{2+} swapping its position from the lattice's tunnels to the $Fe(CN)_6$ vacancies, which eventually may lead to the nucleation of a ZnHCF phase [20]. It has been suggested that such phase transition might have an influence on the ageing of the CuHCF [7,8,11]. It is worth noticing that previous inductively coupled plasma mass spectrometry (ICP-MS) analysis has shown that no appreciable amount of Cu atoms has been found within the aqueous Zn-containing electrolyte, suggesting that no appreciable amount of Cu^{2+} is dissolved upon repeated cycling of the CuHCF [15].

Interestingly, the cycle at which such phase transformation started occurring was different among the various CuHCF electrodes. In particular, a small bump appeared in the differential charge plot of the 50:25, standard (100:50), and 100:100 CuHCF after the 200th cycle (Fig. 3 and SI Section 4 and 5), and in the one of the 200:100 CuHCF after the 300th cycle (SI Section 4). A magnification of the differential charge plots of the 200:100 and 100:100 CuHCF has been included in SI Section 4. Such phase transition occurred at a later stage in the 200:100 CuHCF with respect to the other CuHCF samples, however, this did not ensure a longer cycle life of the material. At the same time, the 200:50 CuHCF reached 80% of its capacity and energy retention in the shortest time among all the synthesised materials without going through such phase-transition at all, as shown from both the galvanostatic profile and the differential charge plot in SI Section 5. Thus, it appears that the occurrence and the consequent development of such two-phase plateau in the galvanostatic profile of the CuHCF may not necessarily have a detrimental effect on the stability and therefore on the ageing of the material.

Interestingly, the two CuHCF powders that showed a longer cycle life, i.e. the 200:100 and especially the 100:100, were the ones with the higher potassium content, as shown from the compositional analysis (6% and 9% normalized K-to-Fe, respectively). Despite the presence of K in the CuHCF structure leads to smaller bond distances in the crystal, and therefore to smaller unit-cell parameters, it does not seem to negatively affect the Zn^{2+} (de-)insertion process. The consequent changes in the electron density of the Fe in the 200:100 and especially 100:100 CuHCF lattice might be responsible for the better electrochemical performance of these materials during their cycle life.

From the electrochemical results it is clear that among the five different CuHCF samples, the initial K-content in the material's lattice does not influence its starting electrochemical performance (Table 1), but rather it has a high impact on its cycle life (Fig. 2a, 2c). For comparison, rhombohedral ZnHCF shows an initial specific charge of 65 mAh g^{-1}, a coulombic efficiency of c.a. 90%, and a cycle life of only 100 cycles at charge/discharge rate of 1C in 1 M $ZnSO_4$ [1]. A graphical comparison of the cycle life of different PBAs at a current rate of 1C can be found within the SI Section 6. It follows that the identification of a strategy to improve the CuHCF performance would certainly be beneficial for the development of long-lasting, cheap and environmentally friendly aqueous Zn-ion batteries, for which further studies are necessary.

4. Conclusions

Despite the great interest that aqueous Zn-ion batteries have recently attracted as energy storage devices for power grid applications, their commercialisation remains hindered by the lack of efficient and green materials for the positive electrode side. Among the members of the Prussian Blue analogues' family, CuHCF is particularly promising as positive electrode material for aqueous ZIBs because of its low costs, non-toxicity, excellent power capability, and relatively simple synthesis route, which could enable the production of larger amounts of material at an industrial scale.

Here, different CuHCF powders have been synthesised in dependence on the variation of the concentration and ratio of the two reactants, i.e. $Cu(NO_3)_2$ and $K_3Fe(CN)_6$, employed during the coprecipitation synthesis, in order to optimise the electrochemical
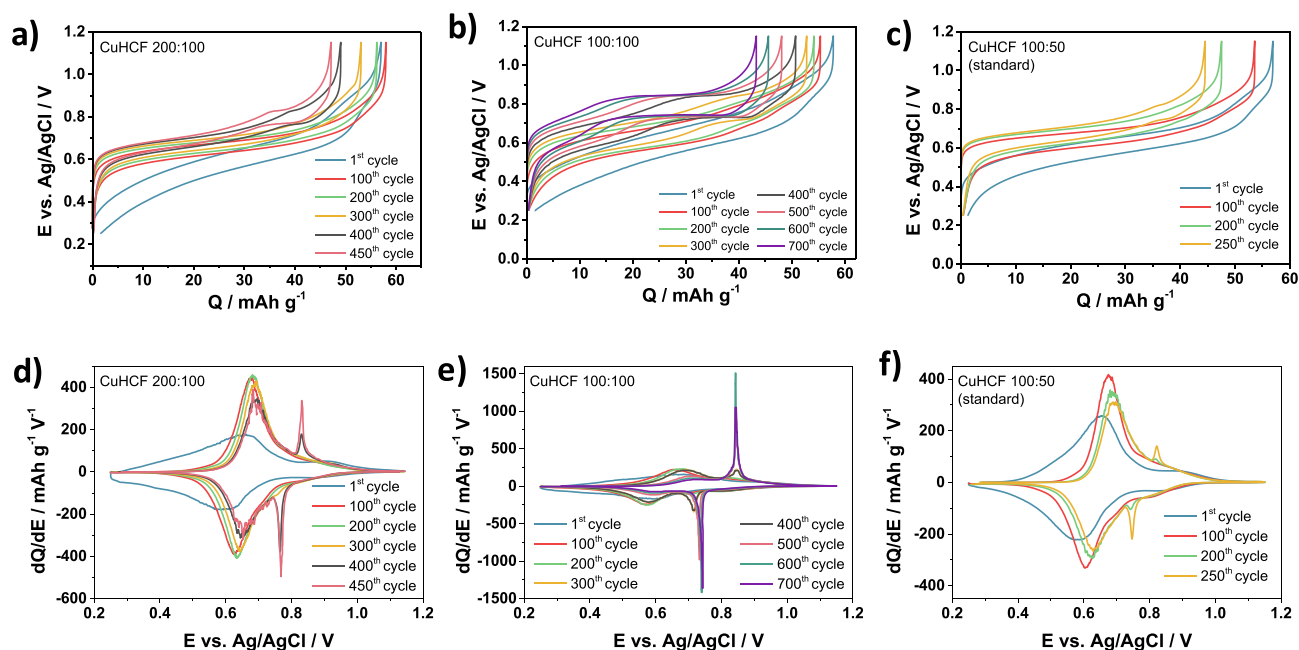
Fig. 3. Galvanostatic cycles (1C rate) and differential charge plots of CuHCF a) d) 200:100, b) e) 100:100 and c) f) 100:50 (standard reactants' concentration), respectively.

performance of the material. No significant change has been observed in terms of particles dimension (around 60–80 nm) and morphology among the different CuHCF powders. However, depending on the reactants' concentration employed during the synthesis, crystallographic and compositional analysis demonstrated that the different pristine CuHCF crystals were characterised by a different potassium content, which changed the bond distances of the lattice, namely: the higher the K-content in the crystal structure, the shorter the bond distances.

Galvanostatic cycling showed that the CuHCF powder with the highest initial K-content in its crystal structure (namely the 100:100) had a longer cycle life, with an energy retention of 80% reached after 800 cycles, contrary to the c.a. 300 cycles of the standard CuHCF.

Further electrochemical, kinetics and post mortem investigation on the aged CuHCF powders will be needed in order to shed light on the mechanism and the morphological and structural changes these materials undergo during their ageing. Such understanding will be vital to further optimise the synthesis parameters and the experimental conditions in order to extend the cycle life of aqueous Zn-ion batteries based on CuHCF.

CRediT authorship contribution statement

Giorgia Zampardi: Conceptualization, Validation, Writing - original draft, Visualization, Project administration, Supervision. **Michael Warnecke:** Investigation, Validation, Writing - review & editing. **Michele Tribbia:** Investigation, Writing - review & editing. **Jens Glenneberg:** Investigation, Writing - review & editing. **Cleis Santos:** Validation, Writing - review & editing. **Fabio La Mantia:** Resources, Conceptualization, Writing - review & editing, Funding acquisition.

Declaration of Competing Interest

The authors declare that they have no known competing financial interests or personal relationships that could have appeared to influence the work reported in this paper.

Acknowledgements

Appendix A. Supplementary data

Supplementary data to this article can be found online at https://doi.org/10.1016/j.elecom.2021.107030.

References

[1] L.Y. Zhang, L. Chen, X.F. Zhou, Z.P. Liu, Towards High-Voltage Aqueous Metal-Ion Batteries Beyond 1.5 V: The Zinc/Zinc Hexacyanoferrate System, Adv. Energy Mater. 5 (2015) 5.

[2] G. Zampardi, F. La Mantia, Prussian blue analogues as aqueous Zn-ion batteries electrodes: Current challenges and future perspectives, Curr. Opin. Electrochem. 21 (2020) 84–92.

[3] Z.G. Yang, J.L. Zhang, M.C.W. Kintner-Meyer, X.C. Lu, D.W. Choi, J.P. Lemmon, J. Liu, Electrochemical Energy Storage for Green Grid, Chem. Rev. 111 (2011) 3577–3613.

[4] V. Blay, R.E. Galian, L.M. Muresan, D. Pankratov, P. Pinyou, G. Zampardi, Research Frontiers in Energy-Related Materials and Applications for 2020–2030, Adv. Sustainable Syst. 4 (2020) 1900145.

[5] A.B. Hashemi, G. Kasiri, J. Glenneberg, F. Langer, R. Kun, F. La Mantia, Electrochemical and Morphological Characterization of Zn-Al-Cu Layered Double Hydroxides as a Negative Electrode in Aqueous Zinc-Ion Batteries, ChemElectroChem 5 (2018) 2073–2079.

[6] G. Zampardi, R.G. Compton, Fast electrodeposition of zinc onto single zinc nanoparticles, J. Solid State Electrochem. (2020).

[7] G. Kasiri, J. Glenneberg, R. Kun, G. Zampardi, F. La Mantia, Microstructural Changes of Prussian Blue Derivatives during Cycling in Zinc-Containing Electrolytes, ChemElectroChem 7 (2020) 3301–3310.

[8] J. Lim, G. Kasiri, R. Sahu, K. Schweinar, K. Hengge, D. Raabe, F. La Mantia, C. Scheu, Irreversible Structural Changes of Copper Hexacyanoferrate Used as a Cathode in Zn-Ion Batteries, Chemistry 26 (2020) 4917–4922.

[9] M. Eckert, W. Peters, J.F. Drillet, Fast Microwave-Assisted Hydrothermal Synthesis of Pure Layered delta-MnO2 for Multivalent Ion Intercalation, Materials 11 (2018) 18.

[10] P. Oberholzer, E. Tervoort, A. Bouzid, A. Pasquarello, D. Kundu, Oxide versus Nonoxide Cathode Materials for Aqueous Zn Batteries: An Insight into the Charge Storage Mechanism and Consequences Thereof, ACS Appl. Mater. Interfaces 11 (2019) 674–682.

[11] R. Trocoli, G. Kasiri, F. La Mantia, Phase transformation of copper hexacyanoferrate (KCuFe(CN)(6)) during zinc insertion: Effect of co-ion intercalation, J. Power Sources 400 (2018) 167–171.

[12] L.Y. Zhang, L. Chen, X.F. Zhou, Z.P. Liu, Morphology-Dependent Electrochemical Performance of Zinc Hexacyanoferrate Cathode for Zinc-Ion Battery, Sci Rep 5 (2015) 11.

[13] F. Scholz, A. Dostal, The Formal Potentials of Solid Metal Hexacyanometalates, Angew. Chem., Int. Ed. Engl. 34 (1996) 2685–2687.

[14] G. Kasiri, J. Glenneberg, A. Bani Hashemi, R. Kun, F. La Mantia, Mixed copper-zinc hexacyanoferrates as cathode materials for aqueous zinc-ion batteries, Energy Storage Mater. 19 (2019) 360–369.

[15] G. Kasiri, R. Trocoli, A.B. Hashemi, F. La Mantia, An electrochemical investigation of the aging of copper hexacyanoferrate during the operation in zinc-ion batteries, Electrochim. Acta 222 (2016) 74–83.

[16] D.O. Ojwang, J. Grins, D. Wardecki, M. Valvo, V. Renman, L. Häggström, T. Ericsson, T. Gustafsson, A. Mahmoud, R.P. Hermann, G. Svensson, Structure Characterization and Properties of K-Containing Copper Hexacyanoferrate, Inorganic Chem. 55 (2016) 5924–5934.

[17] G. Zampardi, S.V. Sokolov, C. Batchelor-McAuley, R.G. Compton, Potassium (De-) insertion Processes in Prussian Blue Particles: Ensemble versus Single Nanoparticle Behaviour, Chem. – A Eur. J. 23 (2017) 14338–14344.

[18] K. Itaya, I. Uchida, V.D. Neff, Electrochemistry of polynuclear transition-metal cyanides - Prussian blue and its analogs, Accounts Chem. Res. 19 (1986) 162–168.

[19] M.B. Soto, F. Scholz, The thermodynamics of the insertion electrochemistry of solid metal hexacyanometallates, J. Electroanal. Chem. 521 (2002) 183–189.

[20] V. Renman, D.O. Ojwang, M. Valvo, C.P. Gomez, T. Gustafsson, G. Svensson, Structural-electrochemical relations in the aqueous copper hexacyanoferrate-zinc system examined by synchrotron X-ray diffraction, J. Power Sources 369 (2017) 146–153.

[21] R. Trocoli, F. La Mantia, An Aqueous Zinc-Ion Battery Based on Copper Hexacyanoferrate, ChemSusChem 8 (2015) 481–485.